European Polymer Journal 46 (2010) 1446–1455

Contents lists available at ScienceDirect

European Polymer Journal

journal homepage: www.elsevier.com/locate/europolj

Macromolecular Nanotechnolgy

Synthesis and characterization of poly(EMA-*co*-HEA)/SiO_2 nanohybrids

A. Vallés-Lluch [a,b,*], J.C. Rodríguez-Hernández [a], G. Gallego Ferrer [a,b,c], M. Monleón Pradas [a,b,c]

[a] Center for Biomaterials and Tissue Engineering, Universidad Politécnica de Valencia, Cno. de Vera s/n, 46022 Valencia, Spain
[b] Regenerative Medicine Unit, Centro de Investigación Príncipe Felipe, Av. Autopista del Saler 16, 46013 Valencia, Spain
[c] Networking Research Center on Bioengineering, Biomaterials and Nanomedicine, Valencia, Spain

ARTICLE INFO

Article history:
Received 10 November 2009
Received in revised form 8 April 2010
Accepted 12 April 2010
Available online 24 April 2010

Keywords:
Nanocomposite
Hybrid
Acrylate
Tetraethyl orthosilicate
Silica
Sol–gel

ABSTRACT

A series of silica-based organic–inorganic nanocomposites, which attempt to mimic the properties of mineralized matrix tissues from natural bone or dentin, have been prepared and characterized as potential candidates for the synthetic matrix of scaffolds for bone or dentin regeneration. The synthesis procedure consisted in the copolymerization of ethyl methacrylate (EMA) and hydroxyethyl acrylate (HEA) during the simultaneous acid-catalyzed sol–gel polymerization of tetraethoxysilane (TEOS) as a silica precursor, giving rise to poly(EMA-*co*-HEA)/SiO_2 nanohybrids with silica contents in the range of 0–30 wt%. Different structures of silica within the organic polymeric matrix were inferred from infrared spectroscopy, energy dispersive X-ray spectroscopy, thermogravimetry, pyrolysis, density assessments, solvent uptake and transmission electron microscopy. TEOS was efficiently hydrolyzed and condensed to silica during the sol–gel process in all cases, and presented a homogeneous distribution in the polymeric matrix, in the form of nanodomains either interdispersed or continuously interpenetrated with the organic network, depending on the silica content. Silica contents above 10% produced co-continuous interpenetrated structures where the silica network reinforces mechanically the organic matrix and at the same time confers bioactivity to the surfaces.

1. Introduction

The incorporation of sol–gel silica derived materials to polymeric matrices constitutes a promising tool to improve mechanical properties or to provide more compatible media for the encapsulation of biological molecules and medicines. The synthesis of hybrids via sol–gel is attractive because of the simplicity and versatility of the sol–gel process, which allows the easy incorporation of a ceramic network into an organic component under mild conditions [1]. The organic–inorganic hybrid materials comprise inorganic networks homogeneously interdispersed or interpenetrated in an organic polymer matrix. In hybrid nanocomposites, the organic and inorganic species are combined at a nanoscale level, i.e., in the form of domains with typical sizes of tens of nanometers [2].

The silica network is expected to reinforce mechanically the organic matrix and at the same time to confer bioactivity to the hybrids. In recent years many works have studied the structure, properties and possible applications of different polymer–silica hybrids, using poly(ε-caprolactone) [3–6], poly(2-hydroxyethyl methacrylate) [7–14], poly(2-hydroxyethyl acrylate) [2,15–18], poly(-methyl methacrylate) [19,20], poly(butyl acrylate) [21], poly(ethylene oxide) [22,23], poly(ethylene oxide-*co*-epichlorhydrin) [24], polyimide [25], polyamide 6,6 [26], poly(vinyl acetate) [27], poly(vinyl alcohol) [28], etc. The organic component is commonly introduced as a precursor, i.e., a monomer or oligomer, and the mineral part with a silica precursor, such as tetraethoxysilane, TEOS. The polymerization of the organic phase proceeds by the free radical reaction of the monomer induced by a thermal- or photo-initiator, during the simultaneous

* Corresponding author at: Center for Biomaterials and Tissue Engineering, Universidad Politécnica de Valencia, Cno. de Vera s/n, 46022 Valencia, Spain. Tel.: +34 963877277; fax: +34 963877276.
E-mail address: avalles@ter.upv.es (A. Vallés-Lluch).

0014-3057/$ - see front matter © 2010 Elsevier Ltd. All rights reserved.
doi:10.1016/j.eurpolymj.2010.04.010

sol–gel polymerization of the silicon alkoxide. This sol–gel process comprises the hydrolysis of the silicon alkoxide to form silanols followed by autocondensation to polymerize into silica polymers, and the aggregation of partially condensed silica molecules to build up the network [1]. These reactions are activated by using either base or acid catalysts, leading, respectively, to favoured hydrolyses and thus large, highly condensed silica particles, or, in the opposite case, to favoured condensations and slightly ramified silica networks and transparent hybrids [2,7,29]. Although hydrolysis and condensations occur concurrently, the relative rate and extent of both reactions and thus the final properties of the materials are affected by the pH, the amount of added water, the hydrophilicity of the polymeric monomer [30], and by the sometimes necessary addition of an alcoholic common solvent to homogenize the solution [31].

In the present work, acrylic monomers have been employed to synthesize and characterize silica-based hybrids, as potential candidates for the synthetic matrix of scaffolds for bone or dentin regeneration. Acrylates have been previously used for biomedical applications because of their good biocompatibility and water permeation characteristics [32–36]. A hydrophobic/hydrophilic copolymer of poly(ethyl methacrylate-*co*-hydroxyethyl acrylate), poly(EMA-*co*-HEA), was selected having in mind that materials aimed to be used for bone or dentin regeneration should satisfy two requirements: good mechanical properties and good interfacial contact with biological fluids. This selected copolymer combines the good mechanical properties provided by the ethyl methacrylate (EMA) component and the hydrophilicity of the hydroxyethyl acrylate (HEA) needed not only for the accessibility of biological fluids into the different porous structures, but also for a good miscibility of the TEOS mixture [2]. A 30 wt% of HEA was sufficient to guarantee mutual solubility. Fig. 1 shows images of poly(EMA-*co*-HEA)/15 wt% SiO_2 scaffolds mimicking natural dentin and after bone-like hydroxyapatite coating. The preparation procedure, characterization, and *in vitro* test of hydroxyapatite deposition are described in detail in a previous work [36].

2. Materials and methods

2.1. Materials

The hybrid nanocomposite materials were obtained by simultaneous polymerization of the organic comonomer mixture and the inorganic silica precursor, similarly as in [7,18]: ethyl methacrylate, EMA (99%, Aldrich) and hydroxyethyl acrylate, HEA (96%, Aldrich), in a 70/30 wt% monomer ratio, were mixed together with a 0.5 wt% of ethylene glycol dimethacrylate, EGDMA (98%, Aldrich), as crosslinking agent and a 2 wt% of benzoyl peroxide, BPO (97%, Fluka), as thermal initiator, relative to monomer weight. Separately, tetraethoxysilane, TEOS, was mixed with distilled water and hydrochloric acid (37%, Aldrich) in the molar ratio 1:2:0.0185, respectively. After 30 min of stirring, both solutions were mixed and stirred for another 30 min. The expected silica content of the nanocomposite samples was adjusted to 0, 5, 10, 15, 20 and 30 wt% by controlling the (EMA + HEA)/TEOS ratio and assuming that the sol–gel reactions were complete. The polymerization reaction was carried out in an oven at 60 °C for 21 h and post-polymerization at 90 °C for 18 h, within moulds consisting in two glass plates with a rubber band in between, in order to obtain sheets 0.8 mm-thick. Then, they were rinsed in a boiling distilled water/ethanol mixture for 24 h to eliminate monomer residues, and eventually allowed to dry in a vacuum desiccator at 80 °C until constant weight. Thus, sheets of poly(ethyl methacrylate-*co*-hydroxyethyl acrylate), poly(EMA-*co*-HEA), 70/30 wt% with varying proportions of silica, SiO_2, up to 30 wt% could

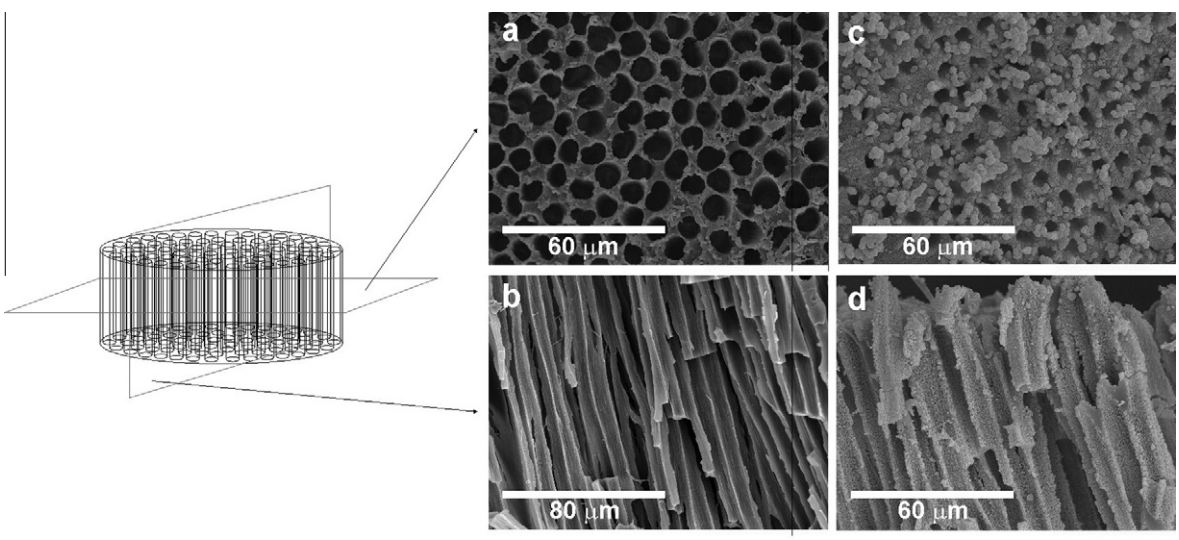

Fig. 1. SEM images of (a) the transversal and (b) longitudinal sections of the poly(EMA-*co*-HEA)/15 wt% SiO_2 scaffolds. (c) and (d) are the same sections after having been coated by bone-like hydroxyapatite directly nucleated from a simulated body fluid (SBF) solution.

Table 1
Sample composition, residue at 700 °C, $w_{700\ °C}$, and SiO_2 content obtained by EDS on the surface and in the bulk, $SiO_{2\ EDS}$.

Sample	Composition	$w_{700\ °C}$ (%)	$SiO_{2\ EDS}$ (%)	
			Surface	Bulk
PEMA	P(EMA)	0.36	–	–
PHEA	P(HEA)	0.92	–	–
H00	P(EMA-*co*-HEA) 70/30 wt%	0.52	0.00	0.00
H05	P(EMA-*co*-HEA) 70/30 wt%–5 wt% SiO_2	4.99	5.18	5.60
H10	P(EMA-*co*-HEA) 70/30 wt%–10 wt% SiO_2	10.64	9.06	8.42
H15	P(EMA-*co*-HEA) 70/30 wt%–15 wt% SiO_2	14.61	15.09	15.33
H20	P(EMA-*co*-HEA) 70/30 wt%–20 wt% SiO_2	19.56	21.21	22.51
H30	P(EMA-*co*-HEA) 70/30 wt%–30 wt% SiO_2	28.70	28.45	24.87

be obtained. Hereafter, these hybrids will be referred to as H*x*, *x* being the percentage of silica. Besides the hybrid materials, sheets of pure poly(ethyl methacrylate), PEMA, and poly(hydroxyethyl acrylate), PHEA, homopolymers were also prepared following the same procedure, as reference systems. The composition of the different samples is given in Table 1.

2.2. Methods

Fourier-transform infrared (FTIR) spectra were collected in a Thermo Nicolet Nexus FTIR spectrometer (Thermo Fischer Scientific Inc., Waltham, MA, USA), in the attenuated total reflection mode (ATR), to determine the surface compositions. The spectra resulted from averages of 128 scans at 4 cm^{-1} resolution, between 650 and 4000 cm^{-1}.

Thermogravimetric analyses (TGA) were carried out to determine the decomposition profiles of the bulk samples, and the decomposition residues. Measurements were done in a TA-SDT Q600 thermobalance (TA Instruments, Newcastle, DE, USA) with approximately 7 mg of sample accurately weighed in standard alumina crucibles. The temperature was raised from 25 to 1000 °C at a rate of 10 °C min^{-1} under a nitrogen flow of 50 ml min^{-1}.

Small pieces of the hybrids with 15% SiO_2 and above were pyrolized in a tubular oven (Gallur, Manises, Spain), programmed with a 3 h-slope to 1000 °C followed by a 4 h-isotherm, under oxygen atmosphere. The obtained residues were analyzed in a JSM-6300 scanning electron microscope (SEM), with the samples previously sputter-coated with gold under vacuum, at 15 kV of acceleration voltage and 15 mm of distance working.

The amount of silica at the surfaces and in the interior of the bulk nanocomposites was quantified by energy dispersive X-ray spectroscopy (EDS) in an Oxford Instruments spectrometer, attached to a JSM-6300 scanning electron microscope (JEOL Ltd., Tokyo, Japan). Samples were previously sputter-coated with carbon under vacuum. Spectra were taken at 10 kV of acceleration voltage and 15 mm of distance working. Silicon was employed as optimization standard. The results presented are the average of three different areas for each nanocomposite.

The carbon, oxygen and silicon amounts could be obtained by EDS on the surfaces and in the bulk (by fracture) of the materials, but the EDS detector cannot reveal the presence of hydrogen. The silica experimental contents, $SiO_{2\ EDS}$, were thus quantified from the silicon average contents through the silica and silicon molar masses, neglecting the amount of hydrogen in the copolymer and in the silanol groups, and the carbon coating of the samples used in the EDS measurements.

A Mettler AE 240 balance (Mettler-Toledo Inc., Columbus, OH, USA) with a sensitivity of 0.01 mg with a Mettler ME 33360 accessory kit was used to measure the density of the bulk samples through Archimedes' principle. The dry samples were weighed in air and immersed in *n*-octane (95%, Fluka, $\rho_{n\text{-octane}} = 0.702\ g\ cm^{-3}$) at room temperature. Each determination was repeated three times per sample.

The density of each sample, ρ, was determined as the ratio of the weight of the sample in air, $m_{in\ air}$, through the volume of *n*-octane displaced, $V_{displaced}$:

$$\rho = \frac{m_{in\ air}}{V_{displaced}} = \frac{m_{in\ air}}{(m_{in\ air} - m_{in\ n\text{-octane}})/\rho_{n\text{-octane}}} \quad (1)$$

where $m_{in\ n\text{-octane}}$ is the weight of the sample immersed in *n*-octane.

The microstructure of the hybrids was observed with a FEI Tecnai Spirit transmission electron microscope (TEM) (FEI Company, Hillsboro, OR, USA) at 60 kV. Samples were previously prepared in a cryogenic ultramicrotome; 60 nm-thick sections were obtained and deposited on a copper grid, pre-coated with a carbon support film. No staining was used to improve contrast.

Swelling of the bulk samples in water and in a water/ethanol 50/50 vol% mixture was quantified at equilibrium, by weighing pieces of dry samples and after equilibration to constant weight at room temperature, using the previously mentioned balance. A constant value of the weight was attained in around 48 h. Measurements were repeated 10 times in water and three times in water/ethanol for each composition.

The equilibrium water content, EWC, is defined as the mass of water, m_{water}, divided by the dry mass of the sample, m_{dry}. Water sorption was also referred to the HEA mass in the sample with the parameter EWC′, defined as:

$$EWC' = \frac{m_{water}}{m_{HEA}} = \frac{m_{water}/m_{dry}}{m_{HEA}/m_{dry}} = \frac{EWC}{x_{HEA}} \quad (2)$$

where x_{HEA} is the mass ratio of HEA in each sample. The water/ethanol equilibrium contents, EWECs, were calculated as mass of solvent uptake, $m_{water\ +\ ethanol}$, divided by the mass of dry sample, m_{dry}. An EWEC′ was also introduced to refer the solvent uptake to the organic phase in the composite, as if solely the organic phase of the material swelled:

$$EWEC' = \frac{m_{water+ethanol}}{m_{copolymer}} = \frac{m_{water+ethanol}/m_{dry}}{m_{copolymer}/m_{dry}} = \frac{EWEC}{x_{copolymer}} \quad (3)$$

In this equation, $x_{copolymer} = (m_{dry} - m_{silica})/m_{dry}$ is the mass ratio of copolymer in the sample.

3. Results

Fig. 2 displays the FTIR spectra of the dry homopolymers and the copolymer. The spectrum of PHEA shows a broad band between 3100 and 3700 cm^{-1}, characteristic of the hydroxyl groups. This band does not appear in the copolymer spectrum. The CH_x asymmetric and symmetric stretching peaks appear at 2962 and 2888 cm^{-1}, respectively, but are less pronounced in the PEMA and H00 spectra. The well defined strong peak at 1700 cm^{-1} appearing in the three spectra corresponds to the C=O bonds of the carboxyl groups. Between 1500 and 650 cm^{-1} the three spectra are quite complex.

Samples of the three compositions were immersed in water for 96 h, and gently surface dried with desiccant paper. Then, the FTIR spectra were obtained, which have also been included in Fig. 2. The broad band between 3700 and 3100 cm^{-1}, as well as the shoulder at 1650 cm^{-1} next to the carbonyl peak characteristic of water, appeared in all cases.

Concerning the nanocomposites' spectra, the broad band assigned to the hydroxyl groups of the copolymer and silanols (3100–3700 cm^{-1}) does not appear, and the C=O stretching peak (1700 cm^{-1}) tends to decrease with increasing silica contents (results not shown). At low wavenumbers, the complex spectrum of the copolymer blurs the silica fingerprint region, so it was decided to subtract it from the spectra of the different nanohybrids. The resulting spectra have been represented in the 1400–600 cm^{-1} range in Fig. 3. The peaks appearing at 1060–1100 and 800 cm^{-1} are attributed to the Si—O—Si asymmetric and symmetric stretching vibration, respectively, and the peak at 950 cm^{-1} is characteristic of the Si—OH stretching vibration of the silica phase [7–9,14,28,37,38]. Their intensities increase proportionally to the silica content.

Hybrid Si—O—C bonds from heterocondensation reactions at organic–inorganic interfaces could also be present (1120–1080 and 836 cm^{-1}), as suggested in the literature [7,38,39], but this cannot be confirmed from the FTIR assays since they overlap the absorption interval of the Si—O—Si bonds.

The residual mass, w, of both homopolymers and the copolymer due to thermal degradation, as well as the derivative curves, dw/dT, are shown in Fig. 4. Decomposition of both PEMA and PHEA polymers seems to take place in two and three main stages, respectively, according to the derivative curves. PEMA decomposes between 210 and 395 °C, whereas PHEA degrades at higher temperatures and more gradually, in the 340–550 °C interval. The copolymer decomposes in the 220–550 °C temperature interval, between the temperatures corresponding to both homopolymers, and exhibits three different degradation steps. At 550 °C, all polymers have totally decomposed without leaving residues.

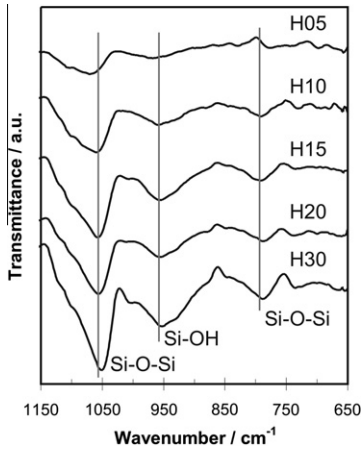

Fig. 3. Resultant FTIR spectra of the hybrid nanocomposites after subtraction of the copolymer spectrum.

The thermogravimetric plots of the silica nanocomposites are displayed in Fig. 5. The weight loss seems to involve initially three main stages. The TGA curves shift to lower temperatures and the overall weight loss decreases as the silica content increases. The first degradation step becomes more pronounced and the second gets smoother, as the derivative curves evidence. At the same time, the last degradation step tends to vanish. The thermogravimetric curves of H15, H20 and H30 samples are quite similar, except for the final residues.

The experimental percentages of residues at 700 °C, $w_{700\ °C}$, have been determined for the different samples

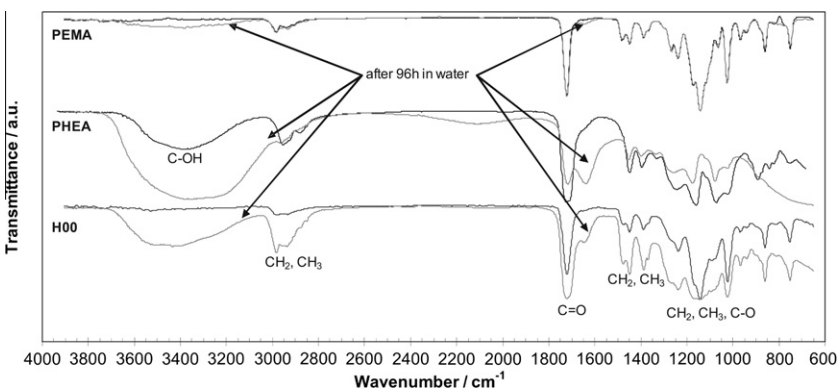

Fig. 2. FTIR spectra of PEMA, PHEA and H00 as dry (—), and after 96 h of immersion in water (—), in the 650–4000 cm^{-1} region.

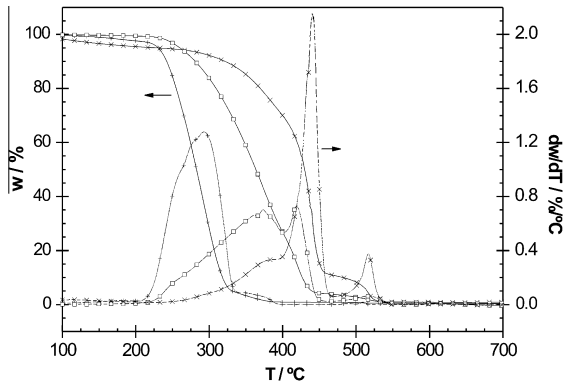

Fig. 4. (—) Residual mass fraction, w = weight loss through initial weight, as a function of temperature and (- -) derivative curves, dw/dT, of: (+) PEMA, (×) PHEA and (□) H00.

and are listed in Table 1. They agree well with the nominal inorganic contents in all cases. For H05 and H10, the residues after the measurements consisted in silica powder. However, for the hybrids with 15 wt% of SiO_2 and above, residues could be removed easily from the crucibles in one piece. This is why only small pieces of hybrids with 15 wt% of SiO_2 and above were pyrolyzed in the tubular oven. Fig. 6 shows the SEM images of the pyrolyzed residues of H15 and H30 fragments. The residues maintained the original shape but shrunk, displaying a smooth surface with occasional cracks.

The silica contents quantified from the Si average contents obtained by EDS, $SiO_{2\ EDS}$, on the surfaces and in the bulk, are displayed in Table 1. The surface and bulk silica percentages are very similar and correlate quite well with the nominal silica contents of the hybrids, despite the limitations of this technique.

The dependence of the density, ρ, of the nanocomposites on the silica content is shown in Fig. 7. The obtained values for PEMA and PHEA polymers are 1.12 and 1.30 g cm^{-3}, respectively. The density increases linearly with the silica content from 1.17 to 1.33 g cm^{-3}.

TEM images given in Fig. 8 lend morphological evidence of the dispersion of silica. The silica phase (dark areas) is uniformly distributed in the nanoscale in all hybrids. Nanohybrids with low percentages of silica display a particle–matrix morphology (small non-interconnected particles dispersed in an organic matrix), which becomes denser with the silica content. Gradually, these aggregates coalesce to produce co-continuous interpenetrated structures where individual silica aggregates are no longer seen. In the H30 sample, the discrete inorganic domains are not detectable.

Fig. 9(a) displays the equilibrium water content of the nanocomposites referred to the dry mass of the sample, EWC, and also referred to the HEA mass in the sample, EWC′. The error bars representing the standard deviation are included. The EWCs for PEMA and PHEA are 1.18% and 202.52%, respectively. The EWC of the copolymer, 8.34%, slightly decreases with the silica content up to 6.74% for H20, and abnormally increases for H30, which was very rigid as dry. The EWC′ do not vary significantly with the amount of silica. The theoretical equilibrium water contents, EWC_{theor}, have been calculated as a linear combination of the specific swelling capacities of both pure homopolymers, and are also represented.

The copolymer and the hybrids are quite rigid and do not absorb water in large quantities or differently. By contrast, ethanol swells significatively the organic phase, even causing the cracking of the nanocomposites with high silica contents. It was therefore decided to swell the nanocomposites in a water/ethanol 50/50 vol% mixture, with the purpose of investigating the influence of silica on the swelling capacity of the copolymer matrix. Fig. 9(b) shows the equilibrium water/ethanol contents for the hybrids referred to the mass of sample, EWECs, and also to the mass of copolymer in the hybrid, EWEC′, considering in the last case that only the organic phase swells. The theoretical water/ethanol equilibrium contents calculated as a linear combination of the specific swelling capacities of both pure homopolymers have also been represented, $EWEC_{theor}$, to compare them with the experimental EWECs. The EWECs for PEMA and PHEA are 33.27% and 225.64%, respectively, and for the copolymer it is 54.00%. The EWEC increases steeply for low silica contents, reaching a maximum somewhere around 5 wt% of silica, which is even higher than the EWEC of PHEA, and decreases progressively afterwards

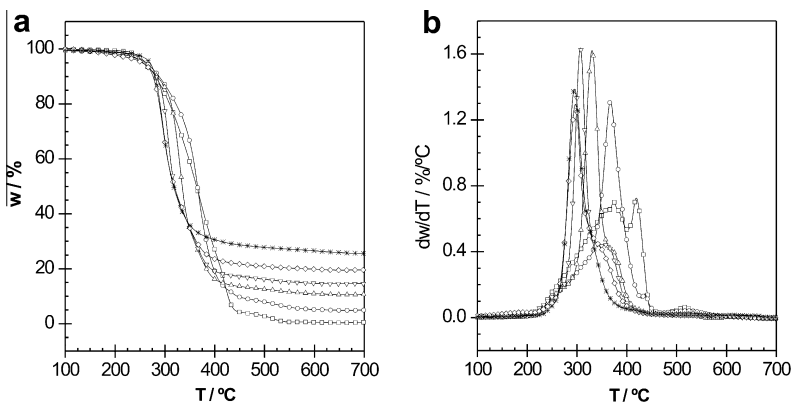

Fig. 5. (a) Residual mass fraction, w = weight loss through initial weight, as a function of temperature and (b) derivative curves, dw/dT, of: (□) H00, (○) H05, (△) H10, (▽) H15, (◇) H20 and (×) H30.

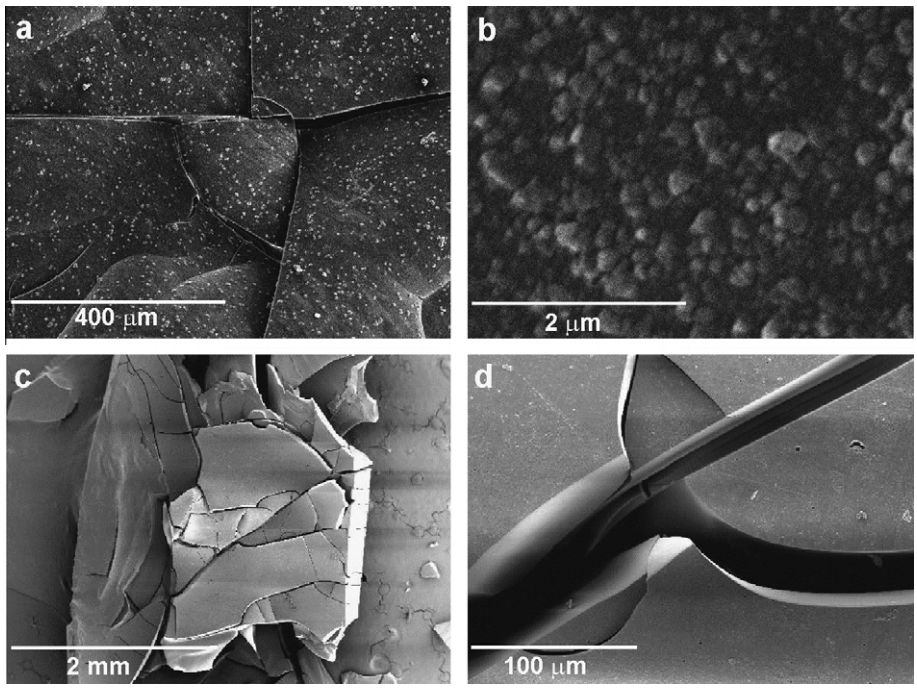

Fig. 6. SEM images of pyrolysis residues of: H15 (a) at 150× and (b) at 30,000×, H30 (c) at 25× and (d) at 400×.

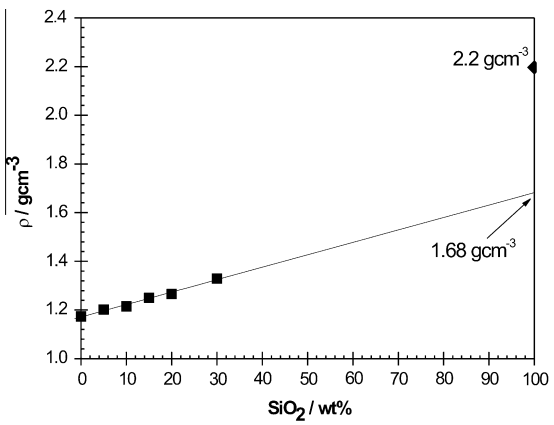

Fig. 7. Density of the nanocomposites, ρ, as a function of the silica percentage.

until a value for H30 somewhat lower than that of PEMA. The EWEC′ curve follows a similar tendency.

4. Discussion

The reaction conditions led to a successful manufacture of hybrid nanocomposites, in spite of the limited miscibility of the EMA monomer and the TEOS. Due to the presence of the OH group of HEA the monomers solution was a good solvent for TEOS and water, and therefore no additional cosolvent was needed [40]. The water/TEOS molar ratio employed was below the stoichiometry of the hydrolysis (2 instead of 4); it was, though, sufficient, since water is also a by-product of the condensation. Thus sheets of hybrid nanocomposites of poly(ethyl methacrylate-*co*-hydroxyethyl acrylate) 70/30 wt%–silica were successfully obtained with varying proportions of silica up to 30 wt%, by the sol–gel method. Silica contents above 30 wt% led to too viscous mixtures hardly injectable in moulds. The samples were optically transparent and increasingly rigid as the percentage of silica increased. This transparency of the composites is an indication of the very small dimensions of the silica phase aggregates: due to the acid catalyzed *in situ* sol–gel synthesis of the silica phase the condensation rate is much greater than the production of silanols by the hydrolysis reaction [1,7], and silica forms as nanometer sized weakly connected or ramified silicate network [1,18,41,42]. Thus, the nanohybrids must consist in two phases, both of them in the form of networks, finely interdispersed or interpenetrated. Optical transparency is conserved if the characteristic phase domain size remains below 400 nm.

The linear increase of the density of the nanohybrids leads to an extrapolated density for a sol–gel 100 wt% SiO_2 of 1.68 g cm^{-3} (Fig. 7), which is between the lower values obtained elsewhere for acid-catalyzed silica gels using higher water/TEOS ratios (1.63–1.32 g cm^{-3} for water/TEOS ratios ranging from 4.2 to 15.3) and the higher value of pure silica glass obtained by curing at 900 °C [1], 2.2 g cm^{-3}. These values indicate that the porous structure of the silica produced by the sol–gel reaction are filled with the organic polymer to a high degree. Rodríguez et al. [18] also observed a high efficient filling of the silica network pores by the organic polymer matrix' chains in PHEA/SiO_2 nanocomposites synthesized by a similar procedure, and attributed this efficient filling to the silica polymerization

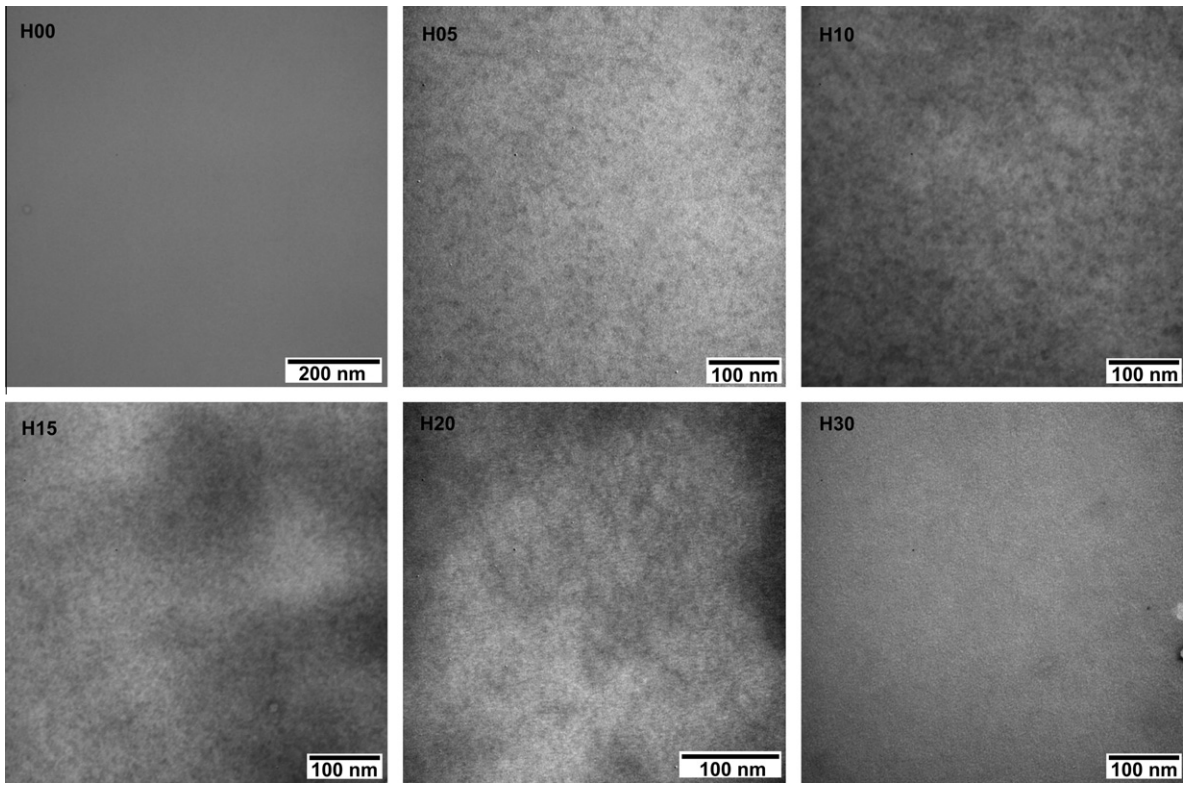

Fig. 8. TEM images of the nanocomposites at 120,000×.

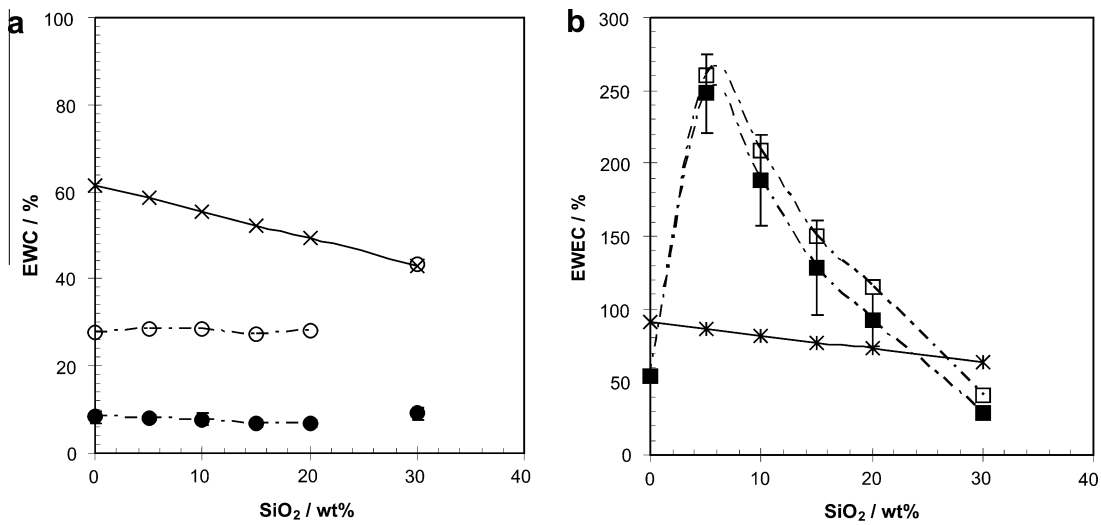

Fig. 9. (a) Equilibrium water contents as a function of the silica contents: (●) referred to the dry mass of the sample, EWC, (○) referred to the HEA mass in the sample, EWC′, (×) predicted from the EWC values of PEMA and PHEA, EWC_{theor}; (b) equilibrium water/ethanol contents as a function of the silica contents: (■) referred to the dry mass of the sample, EWEC, (□) referred to the copolymer mass in the sample, EWEC′, (×) predicted from the EWEC values of PEMA and PHEA, $EWEC_{theor}$.

occurring faster than the organic polymerization and leaving the organic monomer within the spaces developed as the silica structure grows.

According to the literature, the porous structure of silica polymerized via sol–gel is bimodal: a family of small tunnels in the few-nanometer range (around 3 nm) within

the elementary silica particles is produced by the liquids acting as a template during the sol–gel reaction [41,42], and another family of pores consisting in the larger spaces (tens of nanometers) is left between the aggregates of those smaller elementary particles as the phase separation and coalescence of silica proceed to form a continuous network [7,43]. These pores are occupied by the copolymer network.

The infrared spectra of the hybrids, after substracting the overlapped spectrum of the copolymer, reveal the increasing presence of silica on the surfaces as the silica content in them increases. The absence of the broad band characteristic of the OH groups of the silanols or the OH vibrations of HEA can be explained on the basis of the rigidity of the dry samples and consequent imperfect contact with the device. In agreement with the FTIR results, chemical analysis by EDS corroborates that silicon appears at the surface of the nanocomposites in similar amount as in the interior. The good agreement between the percentages of TGA residues, the silica contents obtained by EDS, and the nominal inorganic contents implies that TEOS was efficiently hydrolyzed and condensed to silica during the sol–gel process in all cases, and has a homogeneous distribution in the polymeric matrix. On the one hand, this is of great significance since silica is expected to confer bioactivity to these materials. Silanols at the surface will act as nucleating agents of bone-like apatite crystals when the material will be surrounded by body fluids [5,44,45]. On the other hand, this result excludes a significant dissolution of silica from the surface of the samples during the rinsing with water/ethanol during the manufacturing stage.

The fact that the EWC′ values of the hybrids are almost constant for the different silica contents indicates that the water sorption capacity of the hybrids is due essentially to the HEA component in them, and that this functional unit is as hydrophilic in the nanocomposites as it is in the copolymer, i.e., its individual water affinity is not affected by the increasing presence of silica. Heterocondensation reactions between silica and the organic copolymer, if existent at all, must then involve a negligible number of HEA units.

Pyrolysis changes the structure of the silica network by sintering it to a glass. High magnification of the residues from pyrolysis show structures of aggregated nanoparticles (Fig. 6b). The fact that pyrolized hybrids with silica contents of 15 wt% and above retain the shape and leave a continuous structure demonstrates the high connectivity of the silica phase above 15 wt%. There is clear evidence from the TEM photographs of the hybrids with low silica contents (up to 10 wt%) that the inorganic phase is uniformly dispersed in the form of isolated nanodomains (with average linear dimension about 10 nm), yielding a fine dust after pyrolysis. These silica nanoparticles tend to aggregate in dark larger regions (silica is also detectable in the lighter areas, though). Higher silica contents produce co-continuous interpenetrated structures, where individual silica aggregates are no longer visible. In H30, silica seems to have polymerized to a more perfect interpenetrated network, since discrete inorganic domains are no longer detectable by TEM.

The presence of silica reduces the thermal stability of the nanocomposites, shifting the thermogravimetric curves to lower temperatures. This loss of thermal stability of the silica hybrids was also observed by Costa et al. [9] in PHEMA/SiO_2 composites, who explained it on the basis of a decrease in hydrogen-bonding among copolymer chains promoted by the presence of silica. Other authors [11,46] observed the opposite effect and attributed it to a good homogeneity due to nanoscale mixing and to relatively strong heterogeneous hydrogen bonds tethering silica and polymer chains. On one hand, the decomposition thermograms only seem to be significantly shifted by silica contents below 15 wt%; on the other hand, it is the first weight loss stage which increases in importance. Both circumstances suggest that the high temperatures during the measurements allow condensation reactions between non-condensed silanol groups to start again. Water produced in these condensations could then be involved in an accelerated scission of lateral chains of the organic copolymer during the thermogravimetric assays.

The EWC of the copolymer resembles more that of PEMA than that of PHEA, and is lower than predicted by a simple linear composition rule. The deviation of the EWC from this predicted value can be explained by the fact that the copolymer network is much more rigid (has a higher T_g) than the rubbery PHEA network at ambient temperature, and thus it cannot expand as much as PHEA does while it absorbs water, thus giving rise to this strongly nonlinear swelling. Besides, even though the copolymer swells well in a water/ethanol mixture, its EWEC is still lower than estimated with a linear rule, and more similar to that of PEMA. The abnormally high EWC values of H30 are not reliable and must be attributed to the rigidity and rough surface of the sample, which could have retained some water and falsify the results.

The theoretical equilibrium water/ethanol content obviously decreases slightly and linearly as the percentage of inorganic phase increases. The EWEC values of the hybrids are well above the theoretical ones, and those of EWEC′ follow a similar trend. The increasing relative amount of hydrophilic non-condensed Si—OH terminal groups on the surface of silica disconnected nanodomains, together with the organic network expansion still not hindered by a rigid silica skeleton may account for the initial steep increase in the EWEC′. Between 5 and 10 wt% of silica, a maximum in the EWEC′ is reached, and the later decrease indicates that a continuous silica network interpenetrated with the copolymer network has been developed, in agreement with the integrity of the residues from pyrolysis. The rigid silica skeleton gradually impedes the swelling of the organic chains, which are increasingly constrained. Besides, the increasing connectivity of the silica network is achieved at the expense of terminal silanol groups available for water binding. In the H30 hybrid the silica network is dense and completely continuous throughout the sample, thereby the polymeric matrix swells less than extrapolated, to a degree similar to that of PEMA.

In a different study, these materials were seen to have improved mechanical and bioactive properties [35,47]. The compressive elastic moduli of the nanocomposites

increases from 15 wt% of silica [35], and is expected to increase more in contact with biological fluids, due to hydroxyapatite coating. The presence of silica accelerates the nucleation of hydroxyapatite crystals in an *in vitro* test in simulated body fluid (SBF) [47]. After 7 days, the surfaces of the nanohybrids with intermediate silica contents are completely coated: soluble silicates are released to the solution rendering a surface layer even richer in silanol groups that interact with calcium and phosphate ions inducing the nucleation of hydroxyapatite.

5. Conclusions

Hybrid nanocomposite materials of poly(ethyl methacrylate-*co*-hydroxyethyl acrylate) 70/30 wt%/silica, poly(EMA-*co*-HEA)/SiO_2, were successfully obtained with varying proportions of silica up to 30 wt%. Silica was found to be homogeneously distributed in the polymeric matrix both in the bulk and at the surface. In the hybrids with low silica contents the silica nanodomains were uniformly interdispersed in the organic phase, leaving a relatively high amount of non-condensed surface Si—OH terminal groups, and tended to aggregate into larger regions leaving spaces of tens of nanometers where the organic network occurred. The silica network seemed to percolate and coalesce to form a co-continuous interpenetrated network around 15 wt% of silica content, leaving less hydrophilic terminal silanol groups available and hindering the swelling of the organic phase.

Poly(EMA-*co*-HEA)/SiO_2 nanohybrids with intermediate silica contents (10–20 wt%) present interesting morphologies, with the organic/inorganic phases in the form of interpenetrated networks, where the already formed silica interpenetrated network is expected to reinforce mechanically the organic matrix while it confers bioactivity through its silanol terminal groups exposed at the surface. At the same time, the swelling ability of these composites with intermediate silica contents is still not hindered by a too rigid perfect silica skeleton. The simplicity of the synthesis of these materials offers the possibility of controlling the architecture of the obtained nanocomposites. These features indicate these materials could be of potential use in mineralized tissue regeneration.

Acknowledgements

The authors are grateful to Mario Soriano Navarro and Dr. José Manuel García Verdugo from the Centro de Investigación Príncipe Felipe (Valencia, Spain), where the TEM images were obtained. G.G.F. and M.M.P. acknowledge the support by funds for research in the field of Regenerative Medicine through the collaboration agreement from the Consellería de Sanidad (Generalitat Valenciana), and the Instituto de Salud Carlos III (Ministry of Science and Innovation).

References

[1] Brinker CJ, Keefer KD, Schaefer DW, Ashley CS. Sol–gel transition in simple silicates. J Non-Cryst Solids 1982;48:47–64.
[2] Jackson CL, Bauer BJ, Nakatani AI, Barnes JD. Synthesis of hybrid organic-inorganic materials from interpenetrating polymer network chemistry. Chem Mater 1996;8:727–33.
[3] Tian D, Blacher S, Jerome R. Biodegradable and biocompatible inorganic–organic hybrid materials: 4. Effect of acid content and water content on the incorporation of aliphatic polyesters into silica by the sol–gel process. Polymer 1999;40:951–7.
[4] Rhee SH, Choi JY, Kim HM. Preparation of a bioactive and degradable poly(ε-caprolactone)/silica hybrid through a sol–gel method. Biomaterials 2002;23:4915–21.
[5] Rhee SH. Effect of molecular weight of poly(ε-caprolactone) on interpenetrating network structure, apatite-forming ability, and degradability of poly(ε-caprolactone)/silica nano-hybrid materials. Biomaterials 2003;24:1721–7.
[6] Catauro M, Raucci MG, De Gaetano F, Buri A, Marotta A, Ambrosio L. Sol–gel synthesis, structure and bioactivity of polycaprolactone/$CaO{\cdot}SiO_2$ hybrid material. J Mater Sci Mater Med 2004;15:991–5.
[7] Hajji P, David L, Gerard JF, Pascault JP, Vigier G. Synthesis, structure and morphology of polymer–silica hybrid nanocomposites based on hydroxyethyl methacrylate. J Polym Sci B Polym Phys 1999;37:3172–87.
[8] Lin DJ, Chen CC, Chang CL, Su YC, Cheng LP. Observation of nanoparticles in silica/poly(HEMA) hybrid by electron microscopy. J Polym Res 2002;9:115–8.
[9] Costa ROR, Vasconcelos WL. Structural modification of poly(2-hydroxyethyl methacrylate)–silica hybrids utilizing 3-methacryloxy propyltrimethoxysilane. J Non-Cryst Solids 2002;304:84–91.
[10] Schiraldi C, D'Agostino A, Oliva A, Flamma F, De Rosa A, Apicella A, et al. Development of hybrid materials based on hydroxyethyl methacrylate as supports for improving cell adhesion and proliferation. Biomaterials 2004;25:3645–53.
[11] Lin DJ, Chen CC, Su YC, Huang SH, Cheng LP. Preparation of silica-filled poly(2-hydroxymethyl methacrylate) nanocomposites cured by photoirradiation during the sol–gel process. J Appl Polym Sci 2004;94:1927–35.
[12] Costa ROR, Pereira MM, Lameiras FS, Vasconcelos WL. Apatite formation on poly(2-hydroxyethyl methacrylate)–silica hybrids prepared by sol–gel process. J Mater Sci Mater Med 2005;16:927–32.
[13] Huang SL, Chin WK, Yang WP. Structural characteristics and properties of silica/poly(2-hydroxyethyl methacrylate) (PHEMA) nanocomposites prepared by mixing colloidal silica or tetraethyloxysilane (TEOS) with PHEMA. Polymer 2005;46:1865–77.
[14] Constantini A, Luciani G, Annunziata G, Silvestri B, Branda F. Swelling properties and bioactivity of silica gel/pHEMA nanocomposites. J Mater Sci Mater Med 2006;17:319–25.
[15] Rodríguez Hernández JC, Salmerón Sánchez M, Gómez Ribelles JL, Monleón Pradas M. Polymer–silica nanocomposites prepared by sol–gel technique: nanoindentation and tapping mode AFM studies. Eur Polym J 2007;43:2775–83.
[16] Gómez Tejedor JA, Rodríguez Hernández JC, Gómez Ribelles JL, Monleón Pradas M. Dynamic mechanical relaxation of poly(2-hydroxyethyl acrylate)–silica nanocomposites obtained by the sol–gel method. J Macromol Sci B Phys 2007;46:43–54.
[17] Rodríguez Hernández JC, Serrano Aroca A, Gómez Ribelles JL, Monleón Pradas M. Three-dimensional nanocomposite scaffolds with ordered cylindrical orthogonal pores. J Biomed Mater Res B Appl Biomater 2008;84B:541–9.
[18] Rodríguez Hernández JC, Monleón Pradas M, Gómez Ribelles JL. Properties of poly(2-hydroxyethyl acrylate)–silica nanocomposites obtained by the sol–gel process. J Non-Cryst Solids 2008;354:1900–8.
[19] Li C, Wu J, Zhao J, Zhao D, Fan Q. Effect of inorganic phase on polymeric relaxation dynamics in PMMA/silica hybrids studied by dielectric analysis. Eur Polym J 2004;40:1807–14.
[20] Liu YL, Hsu CY, Hsu KY. Poly(methylmethacrylate)–silica nanocomposites films from surface-functionalized silica nanoparticles. Polymer 2005;46:1851–6.
[21] Costa ROR, Lameiras FS, VAsconcelos WL. Structural control in poly(butyl acrylate)–silica hybrids by modifying polymer–silica interactions. J Sol–Gel Sci Technol 2003;27:343–54.
[22] Takahashi R, Nakanishi K, Soga N. Aggregation behavior of alkoxide-derived silica in sol–gel process in presence of poly(ethylene oxide). J Sol–Gel Sci Technol 2000;17:7–18.
[23] Malucelli G, Priola A, Sangermano M, Amerio E, Zini E, Fabbri E. Hybrid nanocomposites containing silica and PEO segments: preparation through dual-curing process and characterization. Polymer 2005;46:2872–9.

[24] Zoppi RA, Nunes SP. Hybrids of poly(ethylene oxide-*co*-epichlorhydrin) and silica: phase separation, morphology and thermal properties. Polymer 1998;39:6195–203.
[25] Chen Y, Iroh JO. Synthesis and characterization of polyimide/silica hybrid composites. Chem Mater 1999;11:1218–22.
[26] Sengupta R, Bandyopadhyay A, Sabharwal S, Chaki TK, Bhowmick AK. Polyamide 6,6/in situ silica hybrid nanocomposites by sol–gel technique: synthesis, characterization and properties. Polymer 2005;46:3343–54.
[27] Landry CJT, Coltrain BK, Landry MR, Fitzgerald JJ, Long VK. Poly(vinyl acetate)/silica filled materials: material properties of in situ vs fumed silica particles. Macromolecules 1993;26:3702–12.
[28] Pereira MM, Jones JR, Orefice RL, Hench LL. Preparation of bioactive glass-polyvinyl alcohol hybrid foams by the sol–gel method. J Mater Sci Mater Med 2005;16:1045–50.
[29] Pomogailo AD. Polymer sol–gel synthesis of hybrid nanocomposites. Colloid J 2005;67:658–77.
[30] Bandyopadhyay A, Bhowmick AK, De Sarkar M. Synthesis and characterization of acrylic rubber/silica hybrid composites prepared by sol–gel technique. J Appl Polym Sci 2004;93:2579–89.
[31] Mammeri F, Le Bourhis E, Rozes L, Sanchez C. Mechanical properties of hybrid organic–inorganic materials. J Mater Chem 2005;15: 3787–811.
[32] Peppas NA, Hilt JZ, Khademhosseini A, Langer R. Hydrogels in biology and medicine: from molecular principles to bionanotechnology. Adv Mater 2006;18(11):1345–60.
[33] Olmedilla MP, García-Giralt N, Pradas MM, Ruiz PB, Ribelles JLG, Palou EC, et al. Response of human chondrocytes to a non-uniform distribution of hydrophilic domains on poly(ethyl acrylate-*co*-hydroxyethyl methacrylate) copolymers. Biomaterials 2006;27(7): 1012–33.
[34] Gallego Ferrer G, Salmerón Sánchez M, Gómez Ribelles JL, Romero Colomer FJ, Monleón Pradas M. Nanodomains in a hydroplylic–hydrophobic IPN based on poly(2-hydroxyethyl acrylate) and poly(ethyl acrylate). Eur Polym J 2007;43:3136–45.
[35] Vallés Lluch A, Gallego Ferrer G, Monleón Pradas M. Biomimetic apatite coating on P(EMA-*co*-HEA)/SiO_2 hybrid nanocomposites. Polymer 2009;50:2874–84.
[36] Vallés Lluch A, Campillo Fernández A, Gallego Ferrer G, Monleón Pradas M. Bioactive scaffolds mimicking natural dentin structure. J Biomed Mater Res B Appl Biomater 2009;90B:182–94.
[37] Rhee SH, Choi JY, Kim HM. Preparation of a bioactive poly(ε-caprolactone)/silica hybrid through a sol–gel method. Biomaterials 2002;23:4915–21.
[38] Bosch P, del Monte F, Mateo JL, Levy D. Photopolymerization of hydroxyethylmethacrylate in the formation of organic-inorganic hybrid sol–gel matrices. J Polym Sci Polym Chem 1996;34: 3289–96.
[39] Landry CJT, Coltrain BK, Wesson JA, Zumbulyadis N, Lippert JL. In situ polymerization of tetraethoxysilane in poly(methyl methacrylate) – morphology and dynamic-mechanical properties. Polymer 1992;33:1486–95.
[40] Donatti DA, Vollet DR. A calorimetric study of the ultrasound-stimulated hydrolysis of solventless TEOS–water mixtures. J Sol–Gel Sci Technol 1995;4:99–105.
[41] Brinker CJ, Scherer GW. Sol–gel-glass: I. Gelation and gel structure. J Non-Cryst Solids 1985;70:301–22.
[42] Strawbridge I, Craievich AF, James PF. The effect of the H_2O/TEOS ratio on the structure of gels derived by the acid catalysed hydrolysis of tetraethoxysilane. J Non-Cryst Solids 1985;72:139–57.
[43] Yoldas BE. Introduction and effect of structural variations in inorganic polymers and glass networks. J Non-Cryst Solids 1982;51:105–21.
[44] Salinas AJ, Vallet-Regi M, Izquierdo-Barba I. Biomimetic apatite deposition on calcium silicate gel glasses. J Sol–Gel Sci Technol 2001;21:13–25.
[45] Oyane A, Uchida M, Choong C, Triffitt J, Jones J, Ito A. Simple surface modification of poly(ε-caprolactone) for apatite deposition on simulated body fluid. Biomaterials 2005;26:2407–13.
[46] Huang W, Day DD, Kittiratanapiboon K, Rahaman MN. Kinetics and mechanisms of the conversion of silicate (45S5), borate, and borosilicate glasses to hydroxyapatite in dilute phosphate solutions. J Mater Sci Mater Med 2006;17:583–96.
[47] Lluch A Vallés, Ferrer G Gallego, Pradas M Monleón. Effect of the silica content on the physico-chemical and relaxation properties of hybrid polymer/silica nanocomposites of P(EMA- *co* -HEA). Eur Polym J 2010;46:910–7.